Non-linearity of recoil pulse height events in He-3 tubes

M. Manolopoulou [a],*, M. Fragopoulou [a], S. Stoulos [a], W. Westmeier [b], A. Lagogiannis [c], M. Zamani [a]

[a] School of Physics, Aristotle University of Thessaloniki, Thessaloniki 54124, Hellas (Greece)
[b] Philipps-Universität, 35032 Marburg, Germany
[c] N.C.S.R. Demokritos, Ag. Paraskevi Athens 153 10, Hellas (Greece)

ARTICLE INFO

ABSTRACT

Regarding neutron spectrometry, energy calibration of a He-3 counter was performed for neutron energies up to about 7 MeV, for various operating voltages in the proportionality region. Full-energy peak position is linearly correlated with neutron energy, while the position of the ^{3}He recoil peak deviates from a linear response, especially in the lower energy region. By means of the linear full-energy peak calibration, recoil peak energies are found to be significantly lower than those resulting from the kinematics of the reaction. The pulse-height loss is attributed to *initial* recombination. Using the Bragg curve of the recoiling nucleus in the counter gas mixture, it is determined that the pulse-height loss corresponds to a constant portion, 33.5 ± 1.3 %, of the fraction of energy deposited by a ^{3}He nucleus traversing the gas mixture with a stopping power higher than 450 eV/μm. The energy calibration equation for the recoil peaks is derived using the following: (i) the range-energy relation and the stopping power function for a ^{3}He nucleus in the gas mixture where the coefficients of both functions were determined via Monte Carlo calculations, and (ii) the experimentally determined recombination coefficient.

© 2010 Elsevier B.V. All rights reserved.

1. Introduction

^{3}He gas has been widely applied to slow and fast neutron detection and spectrometry due to its high neutron absorption cross-section, chemical inertness and good behaviour in proportional counters with high pressure [1]. When neutrons interact with ^{3}He, three competing reactions have to be considered: ^{3}He(n,p)T, ^{3}He(n,d)D and elastic scattering, each one of which is predominant in a different energy region. The cross-section of the ^{3}He(n,p)T reaction is decreasing from 5330 barns for thermal neutrons, down to 2.6 barns for 56 keV neutrons, where it becomes equal to the elastic scattering cross-section. For high neutron energies, the elastic scattering cross-section becomes larger than that of the (n,p) reaction, and the difference becomes more pronounced with increasing neutron energy. For neutron energies above 4.3 MeV, the (n,d) reaction is also contributing, although the cross-section is an order of magnitude lower than that of the elastic scattering one [2].

For spectrometry applications, a linear energy response of the spectrometry system is expedient. In proportional counters, energy linearity is affected by the general and/or self-induced space-charge effect, the impact of which depends on the gas

amplification, count rate, particle energy at high gas gains, pressure and other characteristics of the counters [3–7]. Recombination effects have also been proposed as an explanation for various effects, such as a count rate-dependent peak shift, an alteration of spectral response or peak shifts observed in Xe-based proportional counters according to radially increasing positions of the primary interactions of γ-rays [8–10].

The non-linearity of pulse height with neutron energy was recorded first for recoiling He nuclei with energies less than 2.6 MeV in gas scintillation counters with a Xe-He mixture, and it was ascribed to the stopping power of alpha particles in the medium [11]. Non-linearity effects were also observed in He-4 spectrometers at low neutron energies, and they were attributed to recombination effects [12]. In a comparative study of He-3 counters using mixtures with Ar or Kr, a distinct difference was found between the experimentally determined recoil peak position in the spectrum and the expected one for neutron energy 2.4 MeV in the counter containing Kr. The deviation became larger as the average Linear Energy Transfer (LET) of the recoiling nucleus was increased above 350 eV/μm [13].

Although recoil peak displacement has been observed sporadically for He-3 tubes, there is a lack of systematic study that could eventually lead to an energy calibration for recoil events. Such a calibration would be advantageous in neutron spectrometry applications because recoil events of high energies could be recorded in the same spectrum area as the events of ^{3}He(n,p)T

reactions of lower energies. In this work, the pulse height produced by the recoiling ^{3}He nuclei is studied as a function of neutron energy and for different operating voltages in a commercially available He-3 counter. Possible reasons for the recoil peak displacement are discussed. The stopping power function of the gas mixture for ^{3}He nuclei, which is calculated via a Monte Carlo method, is used to derive the energy calibration equation for recoil events.

2. Experimental details

The characteristics of the He-3 tube used in this study[1] are: an effective length of 15 cm, a diameter of 5 cm, a cathode material of stainless steel type SS304 and an anode of a tungsten wire with a 25 μm diameter. The filling gas apart from ^{3}He (64.7%) contains Kr (33.3%) as a high stopping-power medium and CO_2 (2%) as quench gas. The overall pressure of the gas mixture is 6 atm (607.95 kPa). The spectrometry system consists of a high-voltage power supply, a charge-sensitive pre-amplifier (Canberra 2006), a Gaussian pulse shape amplifier (Tennelec TC243) and a multichannel analyser (Canberra Multiport II). In addition, a precision pulse generator (Ortec 419) was used for the adjustment of the system.

Irradiations were performed with mono-energetic neutron beams in the energy range from 463 keV to 6.7 MeV provided by a Tandem, Van de Graff accelerator facility at the Institute of Nuclear Physics, NCSR Demokritos, Athens, Hellas. Neutrons with energies in the range of 463 keV to 3.3 MeV were obtained via the ^{7}Li(p,n)^{7}Be reaction. When the projectile energy exceeds 2.2 MeV, besides the neutrons from the ^{7}Li(p,n$_0$)^{7}Be reaction with ^{7}Be at the ground state, a second group of neutrons are also emitted from the ^{7}Li(p,n$_1$)^{7}Be* reaction (first excited state of ^{7}Be, 0.429 MeV) [14]. At projectile energies above 3.68 MeV, neutrons from the ^{7}Li(p,n ^{3}He)^{4}He reaction start contributing to the overall neutron yield, while at energies above 7.06 MeV, neutrons from the ^{7}Li(p,n$_2$)^{7}Be* reaction (second excited state of ^{7}Be) can also contribute to the spectrum. Among these, the n$_1$ neutrons have the highest yield, and at the projectile energies below 5 MeV used in this study, the zero-degree yield of these low-energy neutrons is less than 10% of the n$_0$ neutrons [15]. The peak due to neutrons from the ^{7}Li(p,n$_1$)^{7}Be* reaction is clearly distinguishable from the peak of the main neutron group (n$_0$ neutrons), due to the energy difference between the neutrons emitted from these two reactions [16,17]. Neutron energies in the range of 3.75 to 6.7 MeV were produced via the ^{2}H(d,n)^{3}He reaction. The mean energy loss of the projectile in the target gas cell (window: Mo, 5.1 mg cm^{-2}) was calculated using SRIM/TRIM code [18].

Irradiations were carried out with the anode wire parallel to the projectile beam direction at 0° and a distance between the beam exit and the detector face of 50 cm. Due to the geometrical arrangement of the detector with respect to the projectile beam and because of the solid angle confined from the point of the beam exit by the counter face, neutrons with energies other than the 0° neutron energy can also reach the effective detector volume. In each of the irradiations, the deviation from the 0° neutron energy was calculated by weighing the neutron energies with their intensities at relevant directions. Angular dependences of laboratory cross-sections and energies were calculated using DROSG-2000 code [16]. The calculated difference between the mean neutron energies and the energies of neutrons at 0° was less than 0.2%.

Measurements were carried out at different high-voltage values in the proportionality region of the counter. To compensate

for the different amplification gains that were consequently required, absolute amplification factors of the main amplifier were determined by comparing the amplifier–pre-amplifier triggered pulses produced by thermal neutrons from an Am–Be source with a paraffin moderator. The multichannel analyser was adjusted so that an almost zero offset was achieved for the linear voltage-channel relationship (-0.36 ± 2.1 mV). The amplifier time constant (shaping time) was set at 8 μs, as was optimised in a previous study [17]. The counter was wrapped in 1 mm Cd foil during irradiations to minimise events coming from scattered thermal neutrons. The beam intensity was kept so low that the count rate was about 1000 cps in order to avoid space charge effects in the counter.

3. Results and discussion

Presentations include the following sections: in Section 3.1, the general features of the counter; in Section 3.2, the energy calibration of the peak arising from the ^{3}He(n,p)T reaction; in Section 3.3, the energy calibration for recoil peaks; and finally, in Section 3.4, the equation for energy calibration of recoil events.

3.1. General features of the He-3 counter

In cylindrical proportional counters, the electric field strength per unit pressure (reduced electric field, EF_R) along the radial distance r from the counter axis is as listed below:

$$EF_R = \frac{V}{p \ln(r_b/r_a)} \frac{1}{r}, \tag{1}$$

where r_b and r_α are the cathode and anode radii, respectively, V is the applied voltage and p is the gas pressure. The high field-strength region in which amplification mainly occurs extends typically to a few wire radii, according to r^{-1} dependence. In most of the counter volume, where the ions are created by the primary interactions of the charged particle, the electric field just drifts the ions towards the corresponding electrodes. When the electrons reach the multiplication region ($r \leq r_c$), the development of the Townsend avalanches starts, resulting in a mean multiplication factor or gas gain M given by the following:

$$\ln(M) = \int_{r_a}^{r_c} \alpha(r) \cdot dr, \tag{2}$$

where $\alpha(r)$ is the specific ionisation or first Townsend coefficient [1,4,6]. Several relations have been derived for the gas gain according to the function used for the Townsend coefficient α, which is gas dependent [6,19,20]. Usually, several assumptions are made for simplification, like that the only multiplication process is through electron collision and that recombination, electron attachment to impurities and space charge effects are negligible [1,6,20]. One of the most widely used expressions for M is the Diethorn equation, which was derived assuming the linearity of the specific ionisation with electric field strength and is shown below:

$$\ln(M) = \frac{V}{\ln(r_b/r_a)} \frac{\ln(2)}{\Delta V} \left(\ln \frac{V}{p r_a \ln(r_b/r_a)} - \ln K \right). \tag{3}$$

The constant ΔV corresponds to the potential difference through which an electron moves between successive ionising collisions, while K is the minimum reduced electric field strength required for ionisation [1]. The two parameters can be experimentally determined as constants of the linear relationship fit of $[\ln(M) \cdot \ln(r_b/r_a)/V]$ vs. $[\ln(V/(p \cdot (r_a/ \cdot \ln(r_b/r_a))))]$.

The pre-amplifier pulse amplitude V_{pr} was measured for thermal neutrons from a paraffin-covered Am–Be source, as a

Table 1
Average energy required to produce an ion pair [23], W, and stopping power, S, of a 764 keV proton for pure gases [24].

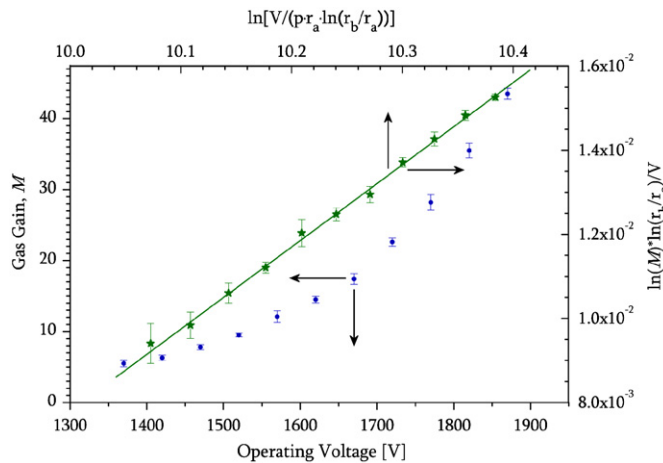|	W [eV/ion pair]	S [MeV cm^2 g^{-1}]
He	42.3	345.7
Kr	24.05	120.4
CO$_2$	32.8	268.2

Fig. 1. Experimental plot of gas gain as a function of operating voltage (left and bottom axes) and $[\ln(M) \cdot \ln(r_b/r_a)/V]$ vs. $[\ln(V/(p \cdot r_a \cdot \ln(r_b/r_a)))]$ (top and right axes). Solid line is the fit to Diethorn equation ($R^2 = 99.93\%$).
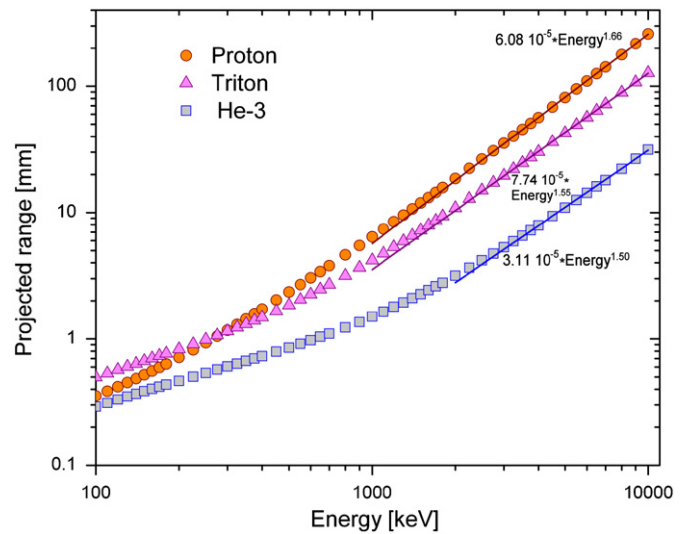

Fig. 2. Calculated ranges of proton, triton and ^{3}He in the counter (points) as a function of their energy. Full lines are fits for energies higher than 1 MeV for proton and triton, and 2 MeV for ^{3}He.

function of the high voltage applied. Amplitude is related to gas gain through the equation: $V_{pr} = NeM/C$, where N is the number of primary ion pairs formed by the charged particle, C is the capacitance of the counter and e is the elementary charge. The number of primary ion pairs created by a particle of energy E is calculated with $N = E/W_m$ where W_m is the average energy spent to produce one ion pair in the gas mixture. The W_m value is calculated to be 37.9 eV according to the expression introduced in ICRU Rep.31, neglecting the quenching gas contribution [21,22]. Values for stopping power (S) and average energy required to produce an ion pair (W) for each of the constituents of the filling gas are presented in Table 1. Gas amplification values measured are in the typical range for ^{3}He neutron-counting applications, varying from 6 to 44 in the proportionality region of the counter. Gas gain as a function of the applied high voltage is presented in Fig. 1. The application of the Diethorn equation for gas gain results in the following parameter estimates: $\Delta V = 35.65 \pm 0.69$ V and $K = 1.471 \times 10^4 \pm 2.3 \times 10^2$ V/(cm atm). The latter indicates that the multiplication region is limited to about two anode radii.

When He-3 counters are irradiated with mono-energetic neutron beams, the resulting pulse height distributions are composed of

i. *The "full energy" peak.* This peak is formed when the total kinetic energy of the ^{3}He(n,p)T reaction products is deposited in the effective gas volume. The reaction is exothermic, with $Q = 764$ keV. Proton and triton share the energy of the reaction, and in the case of thermal neutrons, they are moving in opposite directions, receiving 573 and 191 keV, respectively. Thus, thermal neutrons as well as neutrons with energy less than the Full Width at Half Maximum at 764 keV are recorded in this peak, usually called the *thermal– epithermal* peak. At high energies, the neutron kinetic energy is added to the Q value of the reaction, and the total kinetic energy is

distributed among the two reaction products according to their emission angles in the lab frame. For neutrons with energies above several MeV, the particle ranges become larger than the dimensions of the effective volume of the counter. As a result, a fraction of the energy is deposited to the wall of the counter, the so-called *wall effect*. Therefore, the maximum neutron energy that can form a full energy peak depends on the geometrical characteristics of the counter and the stopping power of the filling gas. Proton and triton ranges for the counter used in this study are presented in Fig. 2, as calculated with SRIM/TRIM code [18]. According to these data, the maximum neutron energy that can form a full energy peak is around 7 MeV, as above this energy, the proton range becomes larger than the effective length of the counter.

ii. *The recoil distribution.* The energy transferred to a nucleus via elastic scattering of a neutron is defined as the following:

$$E_R = \frac{4A}{(1+A)^2} \cos^2\theta \, E_n, \qquad (4)$$

where E_n and E_R are the neutron and recoiling nucleus energies, respectively, A is the ratio of the target nucleus mass to the neutron mass and θ is the scattering angle of the recoiling nucleus in the lab coordinate system [1]. The cross-section of the ^{3}He(n,elastic) reaction is larger than that of ^{3}He(n,p)^{3}H for neutron energies above 56 keV, e.g., it is 2.4 times larger for a 1 MeV neutron energy [2]. As all scattering angles are allowed, in principle, the result in the spectrum is a continuum between a minimum of zero energy and a maximum of whenever the recoiling nucleus is emitted at 0° with respect to the neutron direction. This maximum energy is calculated via equation (4) to be 75% of the neutron energy for the ^{3}He nucleus and to be 29%, 22% and 5% for the C, O and Kr nuclei, respectively. It should be pointed out that although the cross-section of elastic scattering for fast neutrons is larger than the ^{3}He(n,p)T reaction, the result in the pulse height distribution is not so prominent as compared with the full energy peak, due to the distribution of the recoil events over a wide energy region of the spectrum (Fig. 3).

iii. *Gamma-ray distribution.* γ-rays interact mainly with the counter walls and Kr atoms producing electrons. Due to their long range, electrons can deposit a limited amount of energy (usually less than about 200–300 keV) in the counter,

producing pulses with small amplitudes and long rise times. These pulses are recorded in the low-energy region of the pulse height distributions, presenting an exponentially decreasing function of which the exponent is a function of the γ-ray field intensity [1,17,25].

For neutron energies above 4.3 MeV, the ^{3}He(n,d)D reaction contributes to the pulse height distributions, with $Q = -3.27$ MeV. The cross-section of this reaction is from 1 mb at 4.38 MeV to 57.5 mb at 7 MeV (Fig. 3).

3.2. Full energy peak calibration

Pulse height distributions were obtained for 14 neutron energies in the range from 463 keV to 6.7 MeV using five operating voltages between 1500 and 1870 V. With increasing applied voltage, the gas amplification rises exponentially, resulting in higher pulse amplitudes. To compensate the results of varying high voltage, the amplification factor of the main amplifier had to be changed accordingly so that pulses corresponding to the full energy peak had final amplitudes less than the maximum voltage that can be processed by the Analog-to-Digital Converter (ADC, maximum pulse height 10 V). The comparison of the pulse height distributions is accomplished by normalising the spectra to the same amplifier gain, using measured amplification factors. This procedure was considered more appropriate than normalisation of spectra to the centroid of thermal peaks, as the energy distribution of scattered neutrons from the surrounding area was unknown. It should be noted here that as the counter was covered with 1 mm Cd foil, the "thermal" peak registered neutrons with energies above about 1 eV up to several tenths of keV due to system resolution. Some of the reduced pulse height distributions obtained are presented in Fig. 3. Using the above procedure for spectra normalisation, the
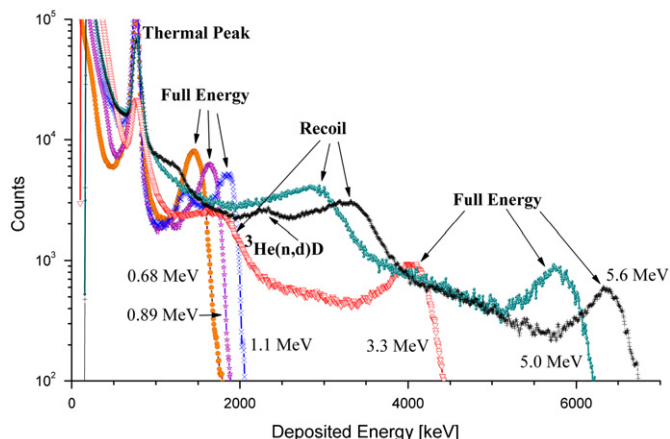
thermal peak centroids of the reduced spectra did not show any significant variation in each applied voltage (Table 2).

While thermal peaks exhibit a Gaussian shape, full energy peaks show an asymmetry that increases with energy at their left/low-energy part, indicative of incomplete charge collection. A similar effect was observed by Loughlin et al. in a He-3 ionisation counter [26] and by Dietz et al. in a He-3 proportional counter [27]. The physical reason for this asymmetry was attributed either to pre-amplifier pulses with long rise times, when protons and tritons are emitted perpendicularly to the anode, or to a space-charge effect. Asymmetry was also observed in the thermal peak during a previous study of the same type of counter as that used in the present work when the operating voltage was increased [17]. In this case, the asymmetry was connected to longer rise time pulses, thus to particles with trajectories almost perpendicular to the anode, and it was attributed to a kind of self-induced space charge effect: when the electron swarm of one of the two particles reaches the multiplication region, it prevents proportional avalanche growth of the second particle.

Full energy peaks were fitted by adding two Gaussian-shaped peaks of different Full Width at Half Maximum (FWHM) to take into account the observed asymmetry. System energy calibrations for the five used operating voltages used are presented in Fig. 4. A linear relationship of deposited energy in the counter with pulse height is observed for a neutron energy up to 6.7 MeV. However, the least squares fitted lines have an offset, a small positive value in channel zero, ranging from 40 to 150 keV with uncertainties from 14% to 46%. As the electronic system was accurately calibrated for zero, this positive offset is indicative of increasing incomplete charge collection with rising deposited energy in the counter. However, due to large uncertainties, no systematic behaviour can be observed with voltage change.

3.3. Recoil peak calibration

Pulse height distributions expected for the recoil energy continua have the same shape as the differential scattering cross-section in the centre-of-mass system, as a result of reaction kinematics [1]. The finite resolution of the system introduces a distortion of this shape, mainly in the area of maximum recoil energy [28]. To estimate the resolution influence on the recoil peak shape, dispersal according to a Gaussian distribution is assumed, and the differential scattering cross-sections are folded with the experimentally determined resolution function using Monte Carlo calculation [2,17]. Some of the calculated results are presented in Fig. 5, illustrating that the recoil peak maximum is expected in the spectrum at a somewhat lower energy than the utmost recoil energy. The difference is decreasing almost linearly from 4.5% to 1.5% for neutrons in the energy region of 1–7 MeV, as the resolution is improved with increasing energy (Table 3).

The recoil peak in the experimental spectrum was fitted using the right part of the peak, including the area around the peak centroid, with a suitable background function: this is linear for $E_n > 1.1$ MeV and exponentially decreasing for the γ-ray contribution in the lower neutron energies. The relation of the recoil peak
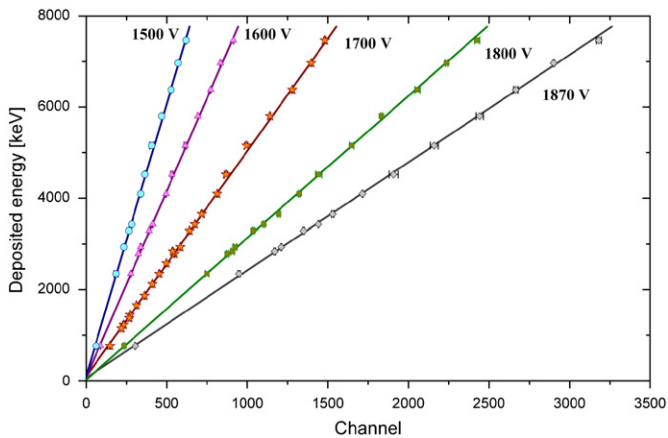

Fig. 3. Pulse height distributions obtained with He-3 counter operating at 1700 V for several neutron energies, normalized to the same amplifier gain.

Table 2
Variation of thermal peak centroid in the reduced spectra for each operating voltage.

High Voltage [V]	Number of spectra	Centroid range: min–max (ch)	Centroid average ± 1 σ (ch)
1500	8	60.30–62.64	61.49 ± 0.90
1600	9	89.94–94.72	91.69 ± 1.54
1700	14	144.62–152.00	148.35 ± 2.73
1800	9	232.78–241.73	235.35 ± 3.32
1870	8	301.37–307.95	305.11 ± 2.92

Fig. 4. Energy calibration of the system by full energy peaks, for several operating voltages. Points correspond to both neutron reactions: ^{3}He(n,p) 3H and ^{3}He(n,d)D.
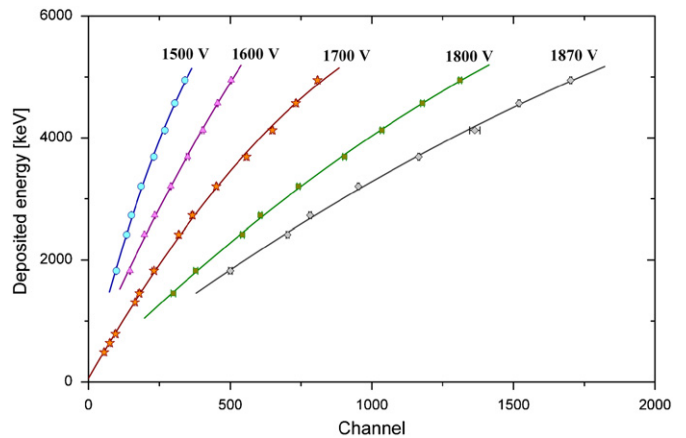

Fig. 6. Energy calibration of the system for recoil peaks at different operating voltages. (Lines are second order polynomial fittings, drawn to guide the eye.)
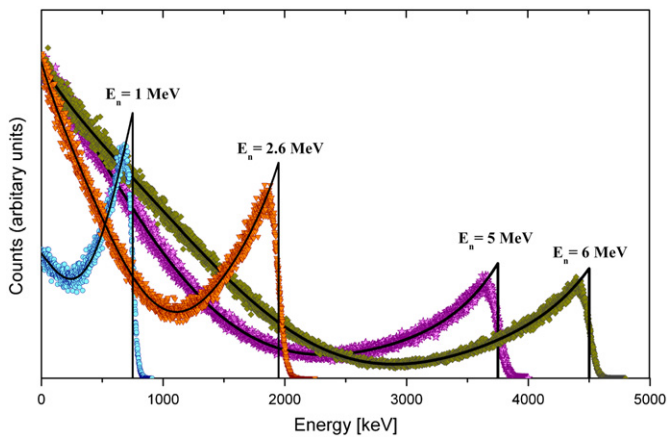

Fig. 5. Resolution effect on the expected ^{3}He recoil distribution shape for different neutron energies (symbols) as calculated with MC using the experimentally determined resolution function. Solid lines are fittings to the angular probability distributions with the Legendre polynomial expansions [2].

Fig. 7. Difference Δp, between expected and measured recoil peak positions as a function of reduced recoil peak energy, for different operating voltages.

Table 3
Difference between maximum ^{3}He recoiled nucleus energy and expected recoil peak energy [MeV], due to resolution influence.

Maximum recoil ^{3}He energy (MeV)	Expected recoil peak energy (MeV)
0.51	0.49
0.67	0.64
0.83	0.79
1.36	1.31
1.51	1.46
1.89	1.82
2.50	2.42
2.82	2.73
3.29	3.20
3.78	3.69
4.21	4.12
4.65	4.57
5.02	4.95

centroid as a function of the reduced energy of recoiling ^{3}He nuclei by the amount calculated as a result of resolution influence (Table 3) is presented in Fig. 6. Non-linear behaviour is observed, at least for lower energies. Similar results were presented for recoil helium peaks in other gas proportional and scintillation counters [12,29].
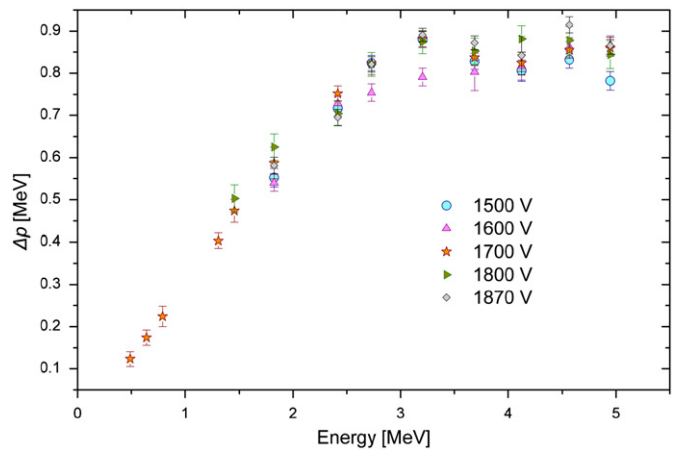
A comparison of the two energy calibrations of the system using full energy or recoil peak shows two distinctly separate curves. For the same deposited energy in the counter, there is a clear deviation between the two pulse heights, with the recoil always smaller than the full energy peak. Pulse height differences measured for different high voltages can be compared by converting them to energy using the corresponding full energy peak calibration of each operating voltage. That difference, denoted as Δp, demonstrates the energy equivalent of the pulse-height loss between the expected and measured recoil peak centroid position in the spectrum. In Fig. 7, Δp is plotted against reduced recoil peak energy due to resolution influence.

Physical reasons that are known causes of pulse-height loss are space charge and recombination effects. In proportional counters, significant space charge effects have been observed at high count rates, as an integrated influence on the gas gain of the positive ions of many discharges as they drift across the counter (the general space charge effect). Also, a space charge effect has been observed when the counter operates in the limited proportionality region (10^7-10^8 electrons in an avalanche) as a self-induced phenomenon that is caused by the large total charge density in the avalanche [3–7,30]. In the latter case, the space charge produced in an avalanche by the preceding electrons in a primary electron cloud is so large that the electric field strength near the anode is weakened, thus reducing the amplification of the following electrons. In the proportionality region and with low

count rates, the space charge effect is considered to be negligible. Both effects are functions of the gas gain. For the He-3 counter used in the present study, the gas gain ranges from 9 to 44 when the operating voltage changes from 1500 to 1870 V (see Section 3.1). The total charge produced in avalanches from protons and tritons, ranges from 10^6 to 8×10^6 electrons for the highest neutron energy measured (6.7 MeV), so the maximum is within the lower boundary of the limited proportionality region. Although such an effect might justify the small positive offset of linear energy calibration (using the full energy peak), the electron density in avalanches of the He-3 counter is expected to be smaller than the respective one produced by photoelectrons used in the studies of the limited proportionality region [7,30], due to large proton, triton and ^{3}He ranges in the counter (several cm, see Fig. 2) instead of several hundreds of μm for photoelectrons. Moreover, as the relative peak shift due to the space charge should be proportional to the gas gain [3] and, as no statistically significant difference was found in Δp with high voltage variation (Fig. 7), the space charge influence on Δp should not be considered as the primary cause.

Recombination, the other known cause of pulse-height reduction, is described by two main processes: the *initial* recombination or *geminate* named after Onsager [31], and the *volume* recombination. In *initial* recombination, a fraction of electrons produced by the primary charged particle are thermalised in the vicinity of their parent ions and, in the absence of an electrical field, have a 100% probability to recombine with them, while even in the presence of a strong electrical field, the *initial* recombination probability does not drop to zero. *Initial* recombination dominates at low count rates, at gas densities of several mg/cm^3 and at electrical field strengths above 1 kV/m [32]. In the *volume* recombination process, electrons thermalised away from their parent ions can recombine with ions of another particle (thus depending on the count rate) or with their parent ions being under random thermal motion. In the case of low count rates, even a small electrical field can remove the electron cloud from the area of their parent ions, reducing the *volume* recombination probability or overcoming it entirely. An extensive discussion of these processes can be found in the works of Bolotnikov and Ramsey [33] and Jaffe et al. [34].

The *volume* recombination process can be excluded as a reason of the reduced pulse height of the ^{3}He recoiling nucleus as compared to pulse heights from proton-to-triton nuclei having the same total kinetic energy, as its influence on both pulse heights should be the same due to the random nature of this process. Moreover, considering the operating conditions of the counter, such as a low count rate and a high electric field above 10 kV/m, volume recombination can be excluded.

In contrast, *initial* recombination is a process that mainly depends on the local ion density and the time that electrons spend in the area of primary ionisation, which in turn, is based on the electric field strength, density and electron mobility in the gas mixture. At a given operating voltage, gas pressure and composition in a counter, the *initial* recombination will therefore depend on the local ion density and the electric field strength in the area of primary ionisation of each particle. In cylindrical counters, the reduced electric field strength is inversely proportional to the radial distance (Eq. (1)); thus, it is expected that pulses from identical particles with the same kinetic energy will undergo different degrees of reduction depending on the radial distance of their electron cloud as well as the orientation of their particle trajectory in respect to the anode. For pulses belonging to the recoil peak, ^{3}He nuclei travelling parallel to the anode at closer distances should undergo less influence from recombination effects than those at larger distances. This results in, besides a general shift of the recoil peak to lower energies, an extra

broadening of the measured distribution, in addition to the broadening caused by other statistical factors that affect the resolution of the counter. Such behaviour has also been reported recently for high pressure proportional counters used for photon detection [10].

The function describing *initial* recombination is expected to vary slowly with electric field strength [33]. With increasing high voltages, less influence should be expected on the final pulse height, thereby reversing the self-induced space charge effect influence. According to the data presented in Fig. 7, no systematic trend was observed concerning differences between the measured and expected recoil peak positions when the operating voltage was increased from 1500 to 1870 V, partially because of the uncertainties involved. The mean values of Δp for different operating voltages and recoil nucleus energies > 1.9 MeV have standard deviations of 3–5%. Therefore, the two competing effects driven by electric field strength cannot account for more than about 5% of the Δp differences observed.

The other factor that affects *initial* recombination probability is the local ion density, which depends on the electronic stopping power of the gas mixture for each type of particle. The two mechanisms by which protons and alpha particles are slowed down in a medium are electronic and nuclear interactions. Nuclear stopping power is important only for low energies, e.g., around 1% for 20 keV protons or 150 keV alphas in water [35]. The stopping power, $S \equiv dE/dx$, of the counter gas mixture for protons, tritons and ^{3}He nuclei was calculated using SRIM Monte Carlo code [18]. Computation was performed for several energies ranging from 0.5 to 10 MeV, with a standard trajectory bin of 20 μm. The calculated stopping power $S(r)$ as a function of ^{3}He nuclei path length, r, was fitted with the following function:

$$S(r) = c_1 \ln \left[c_2 \frac{(d_1-r)+|d_1-r|}{2} + \exp \left[c_2 \frac{(d_1-r)+|d_1-r|}{2} \right] \right] \Big/ ((d_1-r)$$

$$+ |d_1-r|+1) + c_3 \tan h[c_4(r-d_2)] + c_5 \exp \left[1 - \frac{r-d_3}{c_6} - \exp \left[-\frac{r-d_3}{c_6} \right] \right]$$

(5)

where $c_1, ..., c_6$, d_1, d_2 and d_3 are the fitting constants. Eq. (5) was derived empirically for the description of the Bragg-curve shapes. Details regarding the fitting quality are presented in Appendix A.

According to the Bragg curve, charged particles lose energy at higher rates near the end of their trajectories. As the stopping power is increased, the number of ion pairs produced along a particle's path per unit length is increased as well, thereby enhancing the *initial* recombination probability as a result of an increasing ion pair density. Therefore, the recombination influence on pulse height should depend on the fraction of energy deposited at a higher stopping power. If we consider an arbitrary value of stopping power, S_i, the proportion of energy loss at a stopping power greater than S_i, ΔE_i, to the total energy loss of the charged particle, E_0, is given by the equation:

$$\frac{\Delta E_i}{E_0} = \frac{\int_{r_1}^{r_2} S(r)dr}{E_0},$$

(6)

where the limits of the integral, r_1 and r_2, are the solution(s) of Eq. (5) for $S(r)=S_i$.

The ratios $\Delta E_i/E_0$ are calculated for initial energies E_0 in the range from 0.5 to 10 MeV and for stopping power values S_i ranging from 100 eV/μm to the maximum stopping power observed of about 810 eV/μm. Results are presented in Fig. 8. In the same figure, the experimentally measured ratio of $\Delta p/E_0$ is plotted. The

experimental curve has a similar shape as the calculated curves for stopping powers in the region of 400–500 eV/μm.

A more detailed analysis can be performed by examining the ratio of $\Delta p/\Delta E_i$ as a function of ^{3}He ion energy. This ratio is plotted for various stopping power values in Fig. 9. The mean values of $\Delta p/\Delta E_i$ ratios for different stopping power thresholds, S_i, are presented in Table 4. According to these data, the energy equivalent of the pulse height loss, Δp, is a constant fraction of the energy, ΔE_i, deposited at a stopping power higher than about 450 eV/μm.

As already mentioned, the recombination probability is a function of the local ion pair density, which depends on the stopping power $S(E)$. Similar charged particles with different initial kinetic energies in the same traversing medium are slowed down roughly in the same way near the end of their trajectory where the stopping power becomes large, neglecting the energy straggling influence. Therefore, as the stopping power values become similar, the number of charge carriers that undergo recombination is essentially constant and proportional to the energy deposited at a stopping power larger than a critical value S_c, above which the recombination probability becomes signifi-
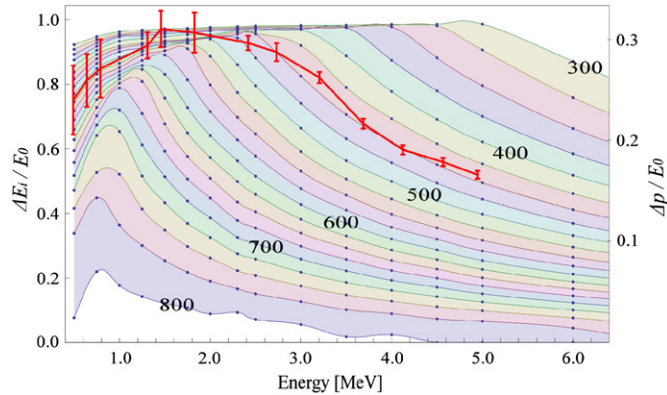

Fig. 8. Ratio $\Delta E_i/E_0$ of the fraction of ^{3}He energy loss with stopping power greater than the indicated values (in eV/μm) as a function of initial energy E_0 of recoiling ^{3}He nucleus (thin lines with small dots, left axis). Curves are calculated in steps of 25 eV/μm. The thick line with error bars presents the experimentally determined $\Delta p/E_0$, as a function of initial energy E_0 (right axis).
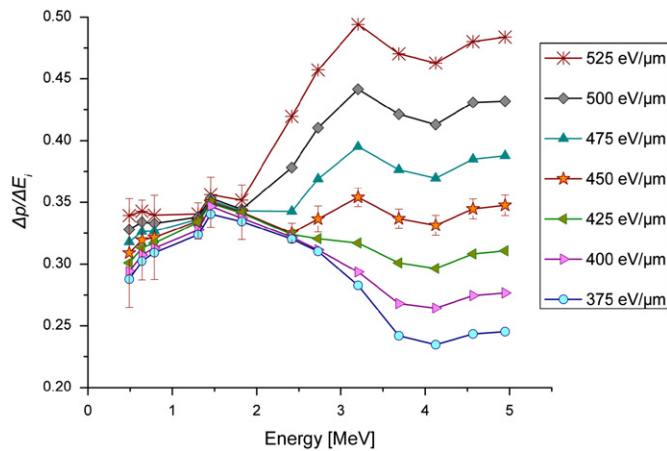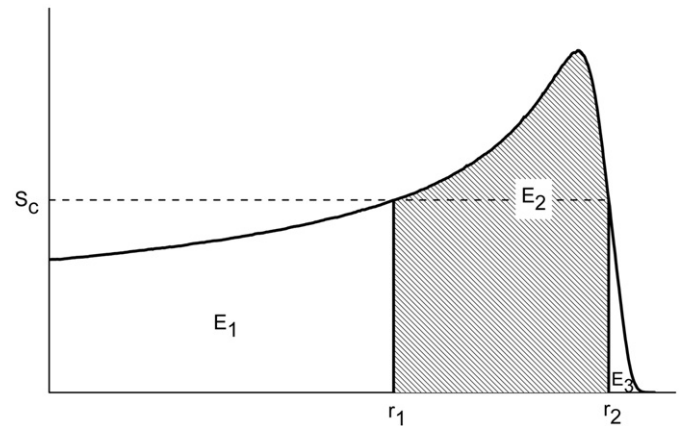

Fig. 10. Sketch of Bragg curve where the dark area, marked with E_2, indicates the part of particle's path where recombination effects become significant.
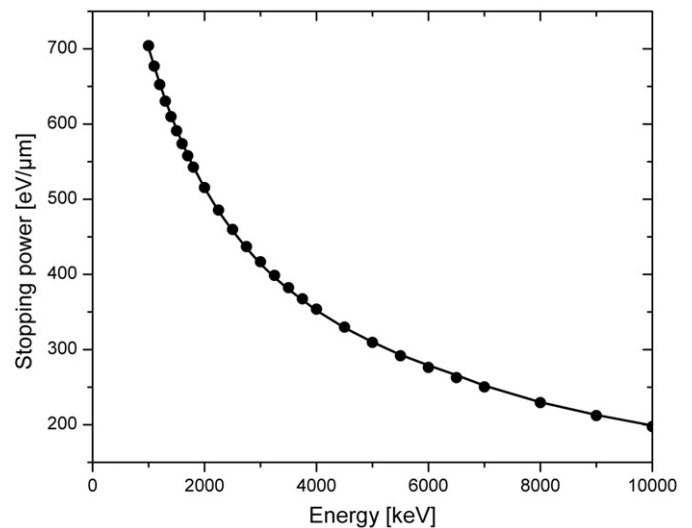

Fig. 9. Ratio of the difference between expected and measured recoil peak position (Δp) to the fraction of energy deposited (ΔE_i) with stopping power larger than the values indicated in the legend, as a function of the initial ^{3}He recoil nucleus energy. The error bars are presented only in one of the curves for presentation clarity.

Fig. 11. Stopping power of ^{3}He nuclei in the counter gas mixture as calculated with SRIM code and fitted with equation (9), $R^2 = 99.986\%$.

Table 4
$\Delta p/\Delta E_i$ percentage for stopping power in the range 400–500 eV/μm.

Energy (MeV)	$\Delta p/\Delta E_i \pm 1\sigma$ [%]				
	> 500 eV/μm	> 475 eV/μm	> 450 eV/μm	> 425 eV/μm	> 400 eV/μm
Average	38.1	35.6	33.5	31.8	30.3
St. Deviation	4.4	2.6	1.3	1.6	2.7

cant. For the counter used in the present study, the results presented in Table 4 indicate that the energy deposited at a stopping power $> 450\,eV/\mu m$ undergoes an integrated recombination defect of $33.5 \pm 1.3\%$. The value of $450\,eV/\mu m$ is larger than the maximum stopping power calculated for protons and tritons, which is about $310\,eV/\mu m$. As a result, no deviation from linearity is observed for the full energy peak calibration.

Evidently, the recombination probability is correlated to ion mobility in the gas mixture. A comparative study of six He-3 counters with different gas mixtures, using Ar or Kr as high-stopping power gases, were irradiated with neutrons of 2.4 MeV and showed a distinct deviation of 14% between the measured and calculated recoil position to the counter containing Kr, while much smaller differences, if any, were observed for Ar gas mixtures [13]. The density normalised thermal electron mobility in Ar is $10 \times 10^{23}\,cm^{-1}\,V^{-1}\,s^{-1}$, while in Kr it is about eight times less, at $1.3 \times 10^{23}\,cm^{-1}\,V^{-1}\,s^{-1}$ [36]. The counter used in the above study differs from the counter used in the present study in its geometrical characteristics and its quench gas (CO_2) concentration, which is 1% instead of 2% here. An increase of the CO_2 concentration in mixtures with Kr reduces electron mobility, e.g. increase in CO_2 concentration from 0.5% to 1% results in about a two-fold reduction in electron mobility [36]. Thus, the almost double deviation of the expected-to-measured recoil peak positions observed in the present study might be attributed to the reduced electron mobility due to an increased CO_2 concentration.

3.4. Energy calibration equation for the recoiling ^{3}He nuclei

The pulse height produced by recoiling ^{3}He nuclei is proportional to the charge carriers that escape recombination:

$$Q = Q_1 + Q_2(1 - R), \tag{7}$$

where $Q_1 + Q_2$ is the total charge initially formed by the ^{3}He recoiling nucleus, Q_2 the charge fraction that is influenced by the recombination effect and R is the recombination coefficient. The charge Q_1 is produced from the energy fraction that is deposited with a stopping power less than S_c, the limit above which recombination effect starts to be significant. This fraction corresponds to the total amounts of energy E_1 plus E_3 of the Bragg curve in Fig. 10, which can be calculated by integrating the Bragg curve within the appropriate limits

$$E_1 = \int_0^{r_1} S(E)dr = \int_{E_0}^{E_c} S(E)\frac{dr}{dE}dE, \tag{8}$$

where the limits of integration are E_0, the initial charged particle energy, and E_c, the energy of which corresponds to a stopping power equal to S_c, $S(E_c) = S_c$.

The stopping power function of alpha particles with energy $< 10\,MeV$ can be expressed by [35]

$$S(E) = (\alpha_3/E)\ln(1 + \alpha_4/E + \alpha_5 E) \tag{9}$$

The range r_0 of any particle with an initial energy E_0 is approximately described by the Bragg–Kleeman rule

$$r_0 = aE_0^p. \tag{10}$$

For alpha particles (also known as the Geiger rule) $p = 1.5$ which is valid for energies above about 1–2 MeV. When an alpha particle has travelled a distance r, its energy has decreased to $E(r)$, which is sufficient to cover the remaining $r_0 - r$ distance

$$r_0 - r = aE(r)^{1.5}$$

and by differentiation

$$\frac{dr}{dE} = -1.5\alpha E^{0.5}. \tag{11}$$

The integral E_1 can be calculated as follows:

$$E_1 = \int_{E_0}^{E_c} S(E)\frac{dr}{dE}dE = \int_{E_0}^{E_c} (\alpha_3/E)\ln(1 + \alpha_4/E + \alpha_5 E)(-1.5\alpha E^{0.5})dE \tag{12}$$

The stopping power of ^{3}He nuclei in the counter gas mixture, $S(E)$, is computed with SRIM code, and constants α_3, α_4 and α_5 are calculated as fitting constants of Eq. (9) (see Fig. 11). Similarly, constant α of the range-energy relationship is calculated to be $(3.115 \pm 0.010)10^{-5}$, where the energy is expressed in keV, and the range is expressed in mm (see Fig. 2).

According to the results presented in Section 3.3, the stopping power above which the recombination effect become significant is $S_c = 450\,eV/\mu m$, which according to Eq. (9) corresponds to $E_c = 2.6\,MeV$. Therefore, when the initial energy E_0 is less than 2.6 MeV, the integral E_1 in Fig. 10 becomes 0 and the charged
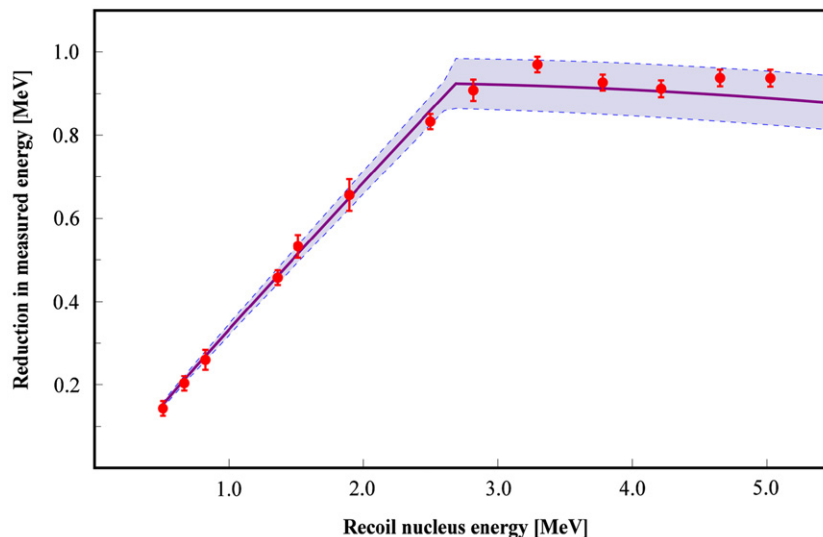

Fig. 12. Calculated reduction (thick line) of recoil ^{3}He nucleus energy with the actually measured reduction (points) as a function of recoil energy. The dark area confines the $\pm 1\sigma$ range of calculated values.

particle is losing all its energy (except the part of the integral marked as E_3), traversing the counter gas with a stopping power larger than $450\,eV/\mu m$. Integral E_3 was calculated with numerical integration of $S(r)$ and appears to be fairly small and constant, at $0.1 \pm 0.01\,MeV$ for initial ^3He ion energies below 7 MeV.

Finally, the recombination defect to recoiling ^3He nuclei pulse height, Δp, can be expressed by the following:

$$\Delta p = \begin{cases} R(E_0 - E_1 - E_3) & E_0 > E_c \\ R(E_0 - E_3) & E_0 \le E_c \end{cases} \tag{13}$$

The analytical expression of Δp is presented in Appendix B.

A comparison of the reduction in the energy of recoil nucleus as it is calculated using Eq. (B.2) and as it is measured is presented in Fig. 12 as a function of ^3He nucleus energy. The presented differences include the influences of both resolution and recombination effects. Experimental points are in the region confined between $\pm 1\sigma$ of the theoretically produced curve. Uncertainty was calculated with the propagation of uncertainties in fitting constants and the recombination coefficient.

4. Conclusions

The experimental results show that the relation of the energy of recoil nuclei vs. pulse height is not a linear function, in contrast to the result observed for the full energy peak. Furthermore, when the recoil nuclei pulse height is converted to energy via energy calibration of the full energy peak, a significantly lower energy than the one expected from kinematics is calculated. The observed variations of the differences between measured and expected recoil nuclei energy with energy and the counter operating voltage, illustrate that the pulse height of recoil nuclei is mostly affected by the *initial* recombination effect. The combined effect of space charge and *initial* recombination variation with electric field strength cannot account for more than about 5% of the measured differences when the operating voltage varies by 20%.

The experimentally determined loss in recoil nuclei energy equivalent to pulse-height loss is a constant fraction of particle energy deposited at a high-stopping power. For the commercially available He-3 counter used in the present study, the fraction of energy deposited at a stopping power larger than $450\,eV/\mu m$ undergoes a recombination defect of $33.5 \pm 1.3\%$.

Regarding spectroscopy applications, in He-3 counters, gas mixtures with Kr as a high stopping power gas were abandoned due to their higher sensitivity for γ-rays, as compared to Ar-based mixtures [37]. The fact that electron mobility is much less important in Kr than in Ar results in increased recombination effects, which move the recoil peak backward towards a lower energy. In this way, a larger area of the spectrum is clear from counts originating from recoil events, which is an advantage for neutron spectroscopy applications.

The energy calibration correction, i.e., the recombination defect, of recoil events in a spectroscopy application can be achieved by Eq. (13). The constants of this equation can be theoretically calculated as constants of the range-energy and stopping power-energy relationships of the recoil nucleus, while the recombination coefficient, R, should be determined experimentally.

Acknowledgments

Appendix A

The stopping power, $S(r)$, was calculated with SRIM/TRIM code as a function of the ^3He nuclei path length and was fitted with Equation (5). The contribution of each term of the function is presented in Fig. 13, in the same sequence as it is written in the equation.

Fitting is performed from $r=0$ up to the point where range straggling influence starts, typically at values of about $< 10\,eV/\mu m$ of the stopping power. Comparison of the total energy loss to ionization as it is computed by SRIM code with the numerically integrated equation (5) is presented in Table 5. Monte Carlo calculated stopping power values (Bragg functions) and the corresponding fitted functions are presented in Fig. 14.
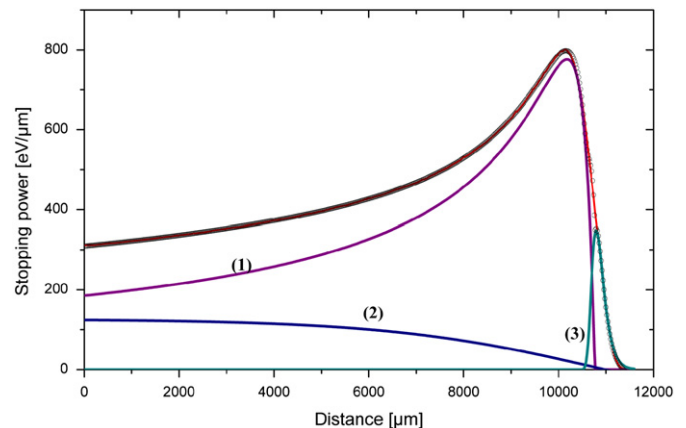

Fig. 13. The contribution of each term of Eq. (5) to the total calculated stopping power (top line) of the counter gas mixture.

Table 5
Comparison of the integrals of the fitting function with the Monte Carlo computed total energy loss to ionization and R-squared of the fitting.

| Initial energy (keV)	Total energy loss to ionization			R^2
	SRIM code	Integral of Eq. (5)	Difference	
0.50	0.493	0.500	−1.31%	0.9997
0.75	0.742	0.749	−0.87%	0.9993
1.00	0.993	0.999	−0.59%	0.9993
1.25	1.243	1.248	−0.45%	0.9990
1.50	1.493	1.496	−0.25%	0.9992
1.75	1.741	1.743	−0.07%	0.9990
2.00	1.992	1.992	0.02%	0.9991
2.30	2.292	2.292	−0.01%	0.9989
2.50	2.492	2.492	0.00%	0.9991
3.00	2.992	2.988	0.12%	0.9990
3.50	3.492	3.485	0.18%	0.9992
4.00	3.991	3.986	0.12%	0.9992
4.50	4.491	4.484	0.16%	0.9993
5.00	4.991	4.981	0.19%	0.9994
6.00	5.990	5.979	0.18%	0.9995
7.00	6.990	6.981	0.12%	0.9994
8.00	7.989	7.979	0.12%	0.9994
9.00	8.989	8.975	0.15%	0.9994
10.00	9.989	9.970	0.19%	0.9992
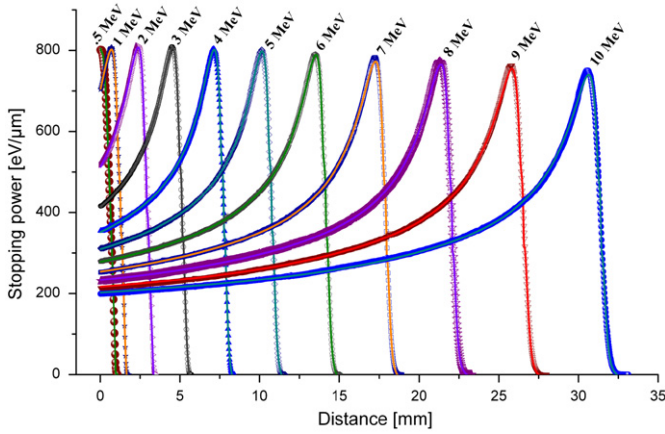
Fig. 14. Bragg curves for ^{3}He nuclei in the counter gas as calculated with SRIM code (points) and the corresponding fitted functions (lines).

Appendix B

The energy E_1, deposited by ^{3}He recoiling nucleus with initial energy E_0, from the beginning of its track up to the point that kinetic energy is reduced to E_c (see Fig. 10), is described by Eq. (12). The integral E_1 was calculated with the program language of Mathematica [38] taking into account the value of the hypergeometric function $F(0.5,0.5,1.5;x^2)=\sin^{-1}(x)/x$.

$$E_1 = 3\frac{\sqrt{2}\alpha\alpha_3}{\sqrt{\alpha_5}}\left\{ \begin{array}{l} \sqrt{1-d}\sin^{-1}\left(\sqrt{\frac{1-d}{1-d+2\alpha_5 E}}\right) \\ + \sqrt{1+d}\sin^{-1}\left(\sqrt{\frac{1+d}{1+d+2\alpha_5 E}}\right) \\ + \sqrt{\frac{\alpha_5}{2}E}\left[2-\ln\left(1+\frac{\alpha_4}{E}+\alpha_5 E\right)\right] \end{array} \right\}\Bigg|_{E_0}^{E_c},$$

$$d = \sqrt{1-4\alpha_4\alpha_5} \tag{B.1}$$

Finally, the pulse height reduction, Δp, due to the recombination effect can be calculated using Eqs. (13) and (B.1) as it follows:

$$\Delta p = \left\{ \begin{array}{ll} R\left(E_0 - \frac{3\sqrt{2}\alpha\alpha_3}{\sqrt{\alpha_5}}\left\{ \begin{array}{l} \sqrt{1-d}\sin^{-1}\left(\sqrt{\frac{1-d}{1-d+2\alpha_5 E}}\right) \\ + \sqrt{1+d}\sin^{-1}\left(\sqrt{\frac{1+d}{1+d+2\alpha_5 E}}\right) \\ - \sqrt{\frac{\alpha_5}{2}E}\left[\ln\left(1+\frac{\alpha_4}{E}+\alpha_5 E\right)-2\right] \end{array} \right\}\Bigg|_{E_0}^{E_c} - E_3\right), & \\ \qquad\qquad R(E_0-E_3) & E_0 \le E_c \\ & E_0 > E_c \end{array} \right.$$

$$d = \sqrt{1-\alpha_4\alpha_5}, \quad E_0 > E_c \tag{B.2}$$

References

[1] G.F. Knoll, Radiation Detection and Measurement, Third Edition, John Wiley & Sons, Inc., New York, 1999.
[2] ENDF/B-VII.0 Evaluated Nuclear Data File. ⟨http://www.nndc.bnl.gov/exfor/endf00.htmwww.nndc.bnl.gov/exfor/endf00.htm⟩.
[3] P.J. Campion, Int. J. App. Rad. Isot. 19 (1968) 219.
[4] R.W. Hendricks, Rev. Sci. Instrum. 40 (1969) 1216.
[5] C. Mori, M. Uno, T. Watanabe, Nucl. Instr. and Meth. 196 (1982) 49.
[6] W. Bambynek, Nucl. Instr. and Meth. 112 (1973) 103.
[7] S. Ito, M. Tosaki, N. Maeda, Nucl. Instr. and Meth. A 368 (1996) 738.
[8] K. Mahesh, Nucl. Instr. and Meth. 133 (1976) 57.
[9] D.J. Grey, R.K. Sood, R.K. Manchanda, Nucl. Instr. and Meth. A 527 (2004) 493.
[10] R.K. Manchanda, R.K. Sood, D.J. Grey, D.J. Isbister, Nucl. Instr. and Meth. A 595 (2008) 605.
[11] J.G. Jenkin, R.E. Shamu, Nucl. Instr. and Meth. 34 (1965) 116.
[12] M. Weyrauch, A. Casnati, P. Schilebeeckx, M. Clapham, Nucl. Instr. and Meth. A 403 (1998) 442.
[13] N. Takeda, K. Kudo, IEEE Trans. Nucl. Sci. 44 (1997) 42.
[14] C.A. Uttley, Neutron Physics and Nuclear data in Science and Technology, vol. 2, Neutron Sources for Basic Physics and Applications, an OECD/NEA report, Pergamon 1983.
[15] S.G. Mashnik, M.B. Chadwick, H.G. Hughes, R.C. Little, R.E. MacFarlane, L.S. Waters and P.G. Young, Los Alamos National Laboratory, (September 1, 2005) available at: ⟨http://arxiv.org/list/nucl-th/0011066⟩.
[16] DROSG-2000: Neutron Source Reactions, Data files with computer codes for 57 accelerator-based neutron source reactions, Version 2.2 (January 2003). M. Drosg, Institute for Experimental Physics, University of Vienna, Austria.
[17] M. Manolopoulou, M. Fragopoulou, S. Stoulos, C. Koukorava, A. Spyrou, G. Perdikakis, S.R. Hashemi-Nezhad, M. Zamani, Nucl. Instr. and Meth. A 562 (2006) 371.
[18] J.F. Ziegler, J.P. Biersack, U. Littmark, Stopping and Ranges of Ions in Matter, Pergamon Press, New York, 1985 See also: SRIM/TRIM The Stopping and Range of Ions in Matter. www.srim.org.
[19] T.Z. Kowalski, Nucl. Instr. and Meth. Phys. Res. A 243 (1986) 501 and the references therein.
[20] J.E. Bateman, Phys. Rep. 375 (2003) 411.
[21] ICRU Rep. 31 "Average energy required to produce an ion pair", 1979.
[22] T.E. Bortner, G.S. Hurst, Phys. Rev. 93 (1954) 1236.
[23] A.V. Zarubin, Nucl. Instr. and Meth. A 283 (1989) 409.
[24] ICRU Rep. 49 , Stopping power and ranges for protons and alpha particles, 1993.
[25] D.H. Beddingfield, N.H. Johnson, H.O. Menlove, Nucl. Instr. and Meth. A 455 (2000) 670.
[26] M.J. Loughlin, J.M. Adams, G. Sadler, Nucl. Instr. and Meth. A 294 (1990) 606.
[27] E. Dietz, M. Matzke, W. Sosaat, G. Urbach, M. Weyrauch, Nucl. Instr. and Meth. A 332 (1993) 521.
[28] A.R. Sayres, K.W. Jones, C.S. Wu, Phys. Rev. 122 (1961) 1853.
[29] J.G. Jenkin, R.E. Shamu, Nucl. Instr. and Meth. 34 (1965) 116.
[30] S. Ito, R. Katano, Y. Isozumi, Nucl. Instr. and Meth. A 324 (1993) 141.
[31] L. Onsager, Phys. Rev. 54 (1938) 554.
[32] N. Golnik, M. Zielczynski, M.A. Gryzinski, P. Tulk, Nucl. Instr and Meth. A 580 (2007) 25.
[33] A. Bolotnikov, B. Ramsey, Nucl. Instr. and Meth. A 428 (1999) 391.
[34] J.E. Jaffe, D.V. Jordan, A.J. Peurrung, Nucl. Instr. and Meth. A 570 (2007) 72.
[35] ICRU Rep. 49, Stopping powers and ranges for protons and alpha particles, 1992.
[36] O.W. Dmitriev, W. Tchorzewska, I. Szamrej, M. Forys, Radiat. Phys. Chem. 40 (1992) 547.
[37] V.E. Krohn Jr., Rev. Sci. Instr. 35 (1964) 853.
[38] Mathematica 4.0, Wolfram Research Inc., USA.